Mathematics Notes

Note 56

August 1977

Pole Measurements for the ATHAMAS Pipe Test

J. T. Cordaro
University of New Mexico
Albuquerque, New Mexico

Abstract

In the ATHAMAS pipe test, surface current and charge density response data were recorded for a metal cylinder illuminated by EMP. Poles and residues describing some of these data have been computed using an iterative technique. Some poles can be identified as corresponding to natural modes of the cylinder. Others match the incident field poles. Most poles in the incident field are shown to be due to ground reflection.

CONTENTS

ILLUSTRATIONS

POLE MEASUREMENTS FOR THE ATHAMAS PIPE TEST

Section 1
INTRODUCTION

In the ATHAMAS Pipe Test, surface current and charge density response data were recorded for a metal cylinder illuminated by EMP. The test objective was to measure the responses of a simple object exposed to ATHAMAS test facility fields and to compare these responses with predictions. According to the Singularity Expansion Method[1] the transient response of a body exposed to EMP can be characterized by the poles and residues of its Laplace transform. These poles and residues in turn are determined by the incident fields and by the body itself. Shumpert[2] and Marin[3] have done theoretical work that can be used to predict cylinder pole locations for the pipe test data. The purpose of this report is to present a method for calculating poles and residues from transient data and to show the results of applying this method to pipe test data.

Section 2
METHOD

Let y_k, k = 1, N, be samples from an observed transient waveform. We want to approximate y_k by a sequence of the form

$$x_k = \sum_{i=1}^{M} C_i \exp(s_i kT), \quad k = 1,\ldots,N \tag{1}$$

where the C_i are the residues and s_i the poles of x_k and T is the sampling interval. For a given choice of the C_i, s_i, and M there may be error between y_k and x_k which we will denote by

$$e_k = y_k - x_k \tag{2}$$

The mean squared error is defined by

$$E(M,c_i,s_i) = \frac{1}{N} \sum_{k=1}^{N} e_k^2 \tag{3}$$

The values of C_i and s_i that minimize the mean squared error for a fixed M are called minimum mean squared error estimates. Within this framework the problem of calculating poles and residues from a transient waveform can be stated in two parts: (1) find the minimum mean squared estimates of C_i and s_i for a fixed M and then (2) determine a "suitable" value for M. The first part of the problem is nontrivial. This can be verified by taking partial derivatives of $E(M,C_i,s_i)$ with respect to C_i and s_i, setting these partials to zero, and observing that the resulting equations are non-linear. The method for finding the C_i and s_i discussed in this report is an iterative technique that attempts to minimize $E(M,C_i,s_i)$ by repeatedly solving linear equations. The second part of the problem is discussed in section 3.

The sequence x_k defined in equation (1) satifies the linear difference equation

$$x_k + a_1 x_{k-1} + \cdots + a_M x_{k-M} = 0 \ , \quad k \geq M+1 \tag{4}$$

The s_i can be found from $Z_i = \exp(s_i T)$ where the Z_i are roots of the characteristic polynomial of the difference equation. So the poles can be computed directly from the a_i. Once the poles are found the residues can be computed by standard least squares techniques. Using equation (2) in equation (4) we get the relation:

$$y_k + a_i y_{k-1} + \cdots + a_M y_{k-M} = e_k + a_1 e_{k-1} + \cdots + a_M e_{k-M} \ , \quad k \geq M+1 \tag{5}$$

Now let v_k be the right hand side of equation (5). With this notation we have the matrix equation:

$$\begin{bmatrix} y_{M+1} \\ \vdots \\ y_N \end{bmatrix} = \begin{bmatrix} -y_M & \cdots & -y_1 \\ \vdots & & \\ -y_{N-1} & \cdots & -y_{N-M} \end{bmatrix} \begin{bmatrix} a_1 \\ \vdots \\ a_M \end{bmatrix} + \begin{bmatrix} v_{M+1} \\ \vdots \\ v_N \end{bmatrix} \tag{6}$$

Let

$$\underline{y} = \begin{bmatrix} y_{M+1} \cdots y_N \end{bmatrix}^T$$

$$h = \begin{bmatrix} -y_M & \cdots & -y_1 \\ \vdots & & \\ -y_{N-1} & \cdots & -y_{N-M} \end{bmatrix} \tag{7}$$

$$\underline{a} = \begin{bmatrix} a_1 \cdots a_M \end{bmatrix}^T$$

$$\underline{v} = \begin{bmatrix} v_{M+1} \cdots v_N \end{bmatrix}^T$$

When using Prony's method one computes the least squares solution of equation (6):

$$\underline{a}_{LS} = (H^T H)^{-1} H^T \underline{y} \qquad (8)$$

This solution is a biased estimate of $\underline{a}$ unless the covariance matrix of $\underline{v}$ is a constant times the identity matrix.[4] In the case considered here the components of $\underline{v}$ are linear combinations of the errors e_k, $k = 1,\ldots,N$. As a result the estimates of a_i are biased and the poles calculated from these estimates can be far from the estimates that minimize $E(M,C_i s_i)$. One way to overcome this problem has been suggested in reference 4 and later in reference 5 in connection with EM work. Reference 4 calls the method "Repeated Least Squares." With it one picks the number of poles M large enough to fit both the signal and noise components of y_k. Doing this tends to "whiten" $\underline{v}$ and remove the bias in the estimate of $\underline{a}$. The author experimented with this Repeated Least Squares version of Prony's method. It gave good results when applied to data sequences with high signal to noise ratios or when enough data points were available that a large number of poles could be used. Unfortunately when analyzing the pipe data, the method had problems pulling the higher frequency poles out of the noise. For this reason, other techniques were investigated. An alternative way of viewing the problem with Prony's method is to notice that the estimate $\underline{a}_{LS}$ minimizes $\underline{v}^T\underline{v}$ which is not the error $E(M,C_i,s_i)$ that we wanted to minimize. To see how the two errors are related we can write the equation for v_k as

$$v_k = e_k + a_1 e_{k-1} + \cdots + a_M e_{k-M} \ , \ k \geq M+1 \qquad (9)$$

Let

$$\underline{e} = \left[e_1 \cdots e_N\right]^T$$

and

$$D = \begin{bmatrix} a_M \cdots a_1 & 1 & 0 \cdots 0 \\ 0 & a_M \; a_1 & 1 & 0 \cdots 0 \\ \vdots & & & \\ 0 \cdots\cdots\cdots & & a_1 & 1 \end{bmatrix} \tag{10}$$

The matrix D is N-M-1 by N. Using these definitions and equation (9) we can write

$$\underline{v} = D\underline{e} \tag{11}$$

The error we would like to minimize is $\underline{e}^T\underline{e} = E(M,C_i,s_i)$. The matrix D is singular so we cannot solve for $\underline{e}$ directly, but by using the pseudo-inverse of D it is easy to show that the minimum norm solution of equation (11) satisfies (see reference 7 for example)

$$\underline{e}^T\underline{e} = \underline{v}^T(DD^T)^{-1}\,\underline{v} \tag{12}$$

We can solve equation (6) for $\underline{v}$ and arrive at

$$\underline{e}^T\underline{e} = (\underline{y} - H\underline{a})^T\,(DD^T)^{-1}\,(\underline{y} - H\underline{a}) \tag{13}$$

This equation expresses the original error defined in equation (3) in terms of the difference equation parameters a_i, $i = 1,\ldots,M$. The problem of minimizing $E(M,C_i,s_i) = \underline{e}^T\underline{e}$ is then the problem of minimizing equation (13) with respect to the a_i. Notice that the poles and residues do not appear directly in equation (13). The equation is non-linear but a simple iterative technique can be used to find the minimum. The relationship between $\underline{e}$ and $\underline{v}$ and the iterative technique discussed below are contained in reference 6.

We can get equation (13) with a statistics argument too. Suppose $\underline{e}$ is a vector of uncorrelated random variables each with mean zero and variance one. Then from equation (11) the covariance of $\underline{v}$, R_v will be

$$R_v = DD^T \tag{14}$$

Using this expression for R_v we can see that the minimum variance, unbiased estimate for $\underline{a}$ is given by equation (13). Incidently, equation (14) shows that the Prony's method estimates will be biased unless $a_i = 0$, $i = 1,\ldots,M$.

To motivate the technique for minimizing equation (13), we observe that if the matrix DD^T did not depend on $\underline{a}$ then the minimum of $\underline{e}^T\underline{e}$ would be given by the solution for $\underline{a}$ from the normal equations.

$$H^T(DD^T)^{-1}H\underline{a} = H^T(DD^T)^{-1}\, y \tag{15}$$

Since D does in fact depend on $\underline{a}$ we can use equation (15) but with iterations. That is, we solve 15 for $\underline{a}$ with DD^T = identity matrix. Then compute DD^T from the estimated $\underline{a}$ and recompute $\underline{a}$ from equation (15). This process is continued until the estimate of $\underline{a}$ converges.

Equation (15) shows the inverse of DD^T. It is unnecessary and inefficient to compute this inverse. Since DD^T is a symmetric, positive definite matrix, it can be factored with Cholesky's method[7] as

$$DD^T = F^TF \tag{16}$$

Where F is upper triangular and non-singular. Define $\tilde{\underline{y}}$ and $\tilde{H}$ as solutions of the equations

$$F^T\tilde{\underline{y}} = \underline{y} \tag{17}$$

$$F^T\tilde{H} = H$$

Using equations (17) in equation (15) we can get

$$\tilde{H}^T\tilde{H}\underline{a} = \tilde{H}^T\tilde{\underline{y}} \tag{18}$$

as the set of normal equations to be solved for $\underline{a}$.

To summarize, the iterative procedure consists of the following steps:

1. Solve equation (15) for $\underline{a}$ with $DD^T = I$.
2. Compute DD^T from the present $\underline{a}$.
3. Factor DD^T and compute $\tilde{\underline{y}}$ and $\tilde{H}$.
4. Solve for a new $\underline{a}$ from equation (18).
5. Check if the new $\underline{a}$ has changed appreciably from the previous one. If yes, return to step 2. Otherwise the iteration is complete.

Since this technique involves iteratively premultiplying and solving linear equations, we will call it the iterative premultiply method. Unfortunately the method does not converge to the true minimum of equation (13). This can be verified by computing the gradient of $\underline{e}^T\underline{e}$ with respect to $\underline{a}$. The normal equations (15) come from taking the gradient of $\underline{e}^T\underline{e}$ while holding DD^T constant. The two sets of equations are not identical and as a result the parameter estimates are not the same. Reference 6 has an example that illustrates this fact. Our experience has been that when the data sequence y_k, $k = 1,\ldots,N$ consists of a sum of complex exponentials plus noise the method works very well. If however y_k is not of this form, for example if y_k had a triangular shape, then it is worthwhile to go to a different iterative technique to get to the true minimum of $\underline{e}^T\underline{e}$.

There is another way of doing the calculation in the iterative technique that should be mentioned. The iterative prefilter method[8,9] is very similar to the iterative premultiply technique discussed here. We wrote a program to implement this method. It executes much faster than the premultiply method but does not appear to be as numerically stable. We were not able to increase the system order M to as large values as with the premultiply method and still have the iterations converge. However, when both techniques converge they give identical results. We expect to continue work on the iterative prefilter method since it is faster and uses less computer memory.

The iterative premultiply method has been tested on computer generated data and pipe data. It gives more accurate results than Prony's method when used on computer generated data. When used on the pipe data it has been able to find high frequency poles in cases where Prony's method failed. For these reasons the iterative premultiply method was used in the data analysis reported in the next section.

Section 3
RESULTS

Transient data waveforms from the Pipe Test were recorded and then digitized on Tektronix 7912 transient digitizers. For many waveforms the early time response was recorded on one scope and late time response on another. The resulting digitized waveforms were time tied and stored in the DASET system data files. Our analysis of a record began by taking it from the DASET files and interpolating it to yield the evenly spaced samples y_k, $k = 1,\ldots,N$, referred to in the last section.

In this report we compare the poles found from data with the pipe in four different locations: 00,01,00 and 00,10,00 both directly under the pulser and 00,01,30, and 00,10,30 at 30 meters along the Z-axis (see figure 1). The data at the Z = 00 locations are records of the derivative of axial current. The data at the Z = 30 locations are records of waveforms that have been integrated as part of the instrumentation and as a result are records of the axial current itself. At each location the pipe's longitudinal axis was parallel to the X-Y plane. The center of this axis was located at X = 00. The sensor was located on top of the pipe at 0.25 m in the +X direction.

The first records analyzed consist of fourteen shots at 00, 01, 00. The graph of a typical shot is shown in figure 2. The corresponding Fourier transform magnitude is in figure 3. The first couple of peaks in the time domain graph are due to the pulser and not the pipe response. To avoid finding poles from these early time peaks, the iterative premultiply method was applied to the record starting at 150 ns. Several combinations of sampling interval T, number of points N, and system order M were tried. Only one pair of poles that was numerically stable could be found. It is interesting to look at figure 3 in this regard. The pole pair found corresponds to the peak near 10 MHz. The peaks around 100 MHz are due to the pulser and were reduced by starting the

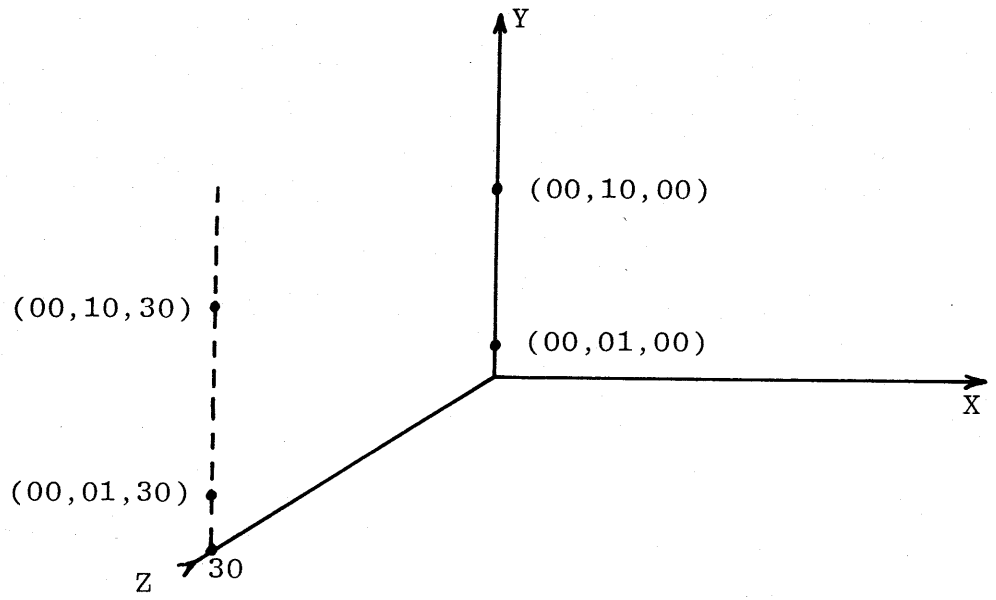

Figure 1. Four Pipe Locations Analyzed

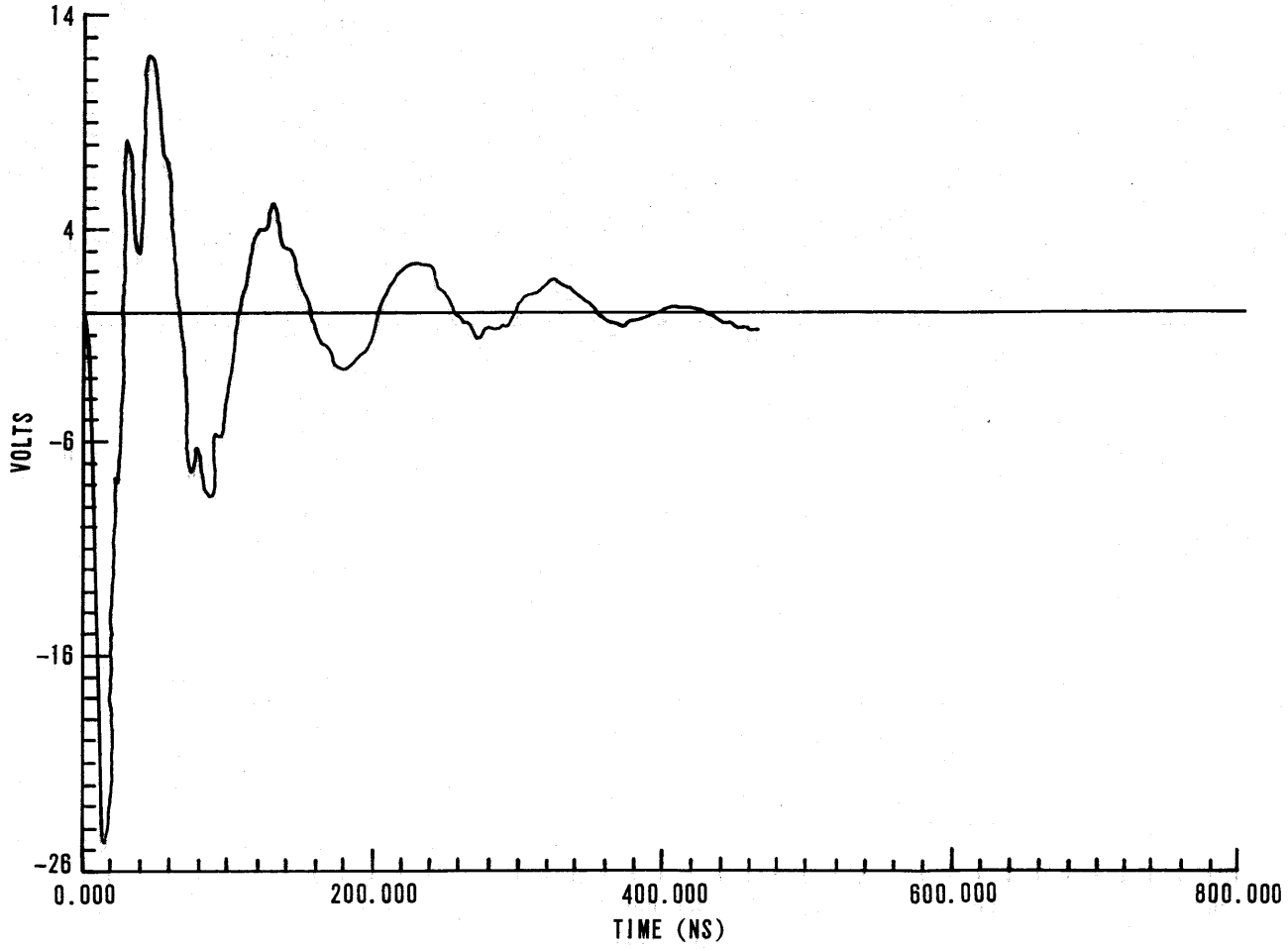

Figure 2. Reponse at 00,01,00

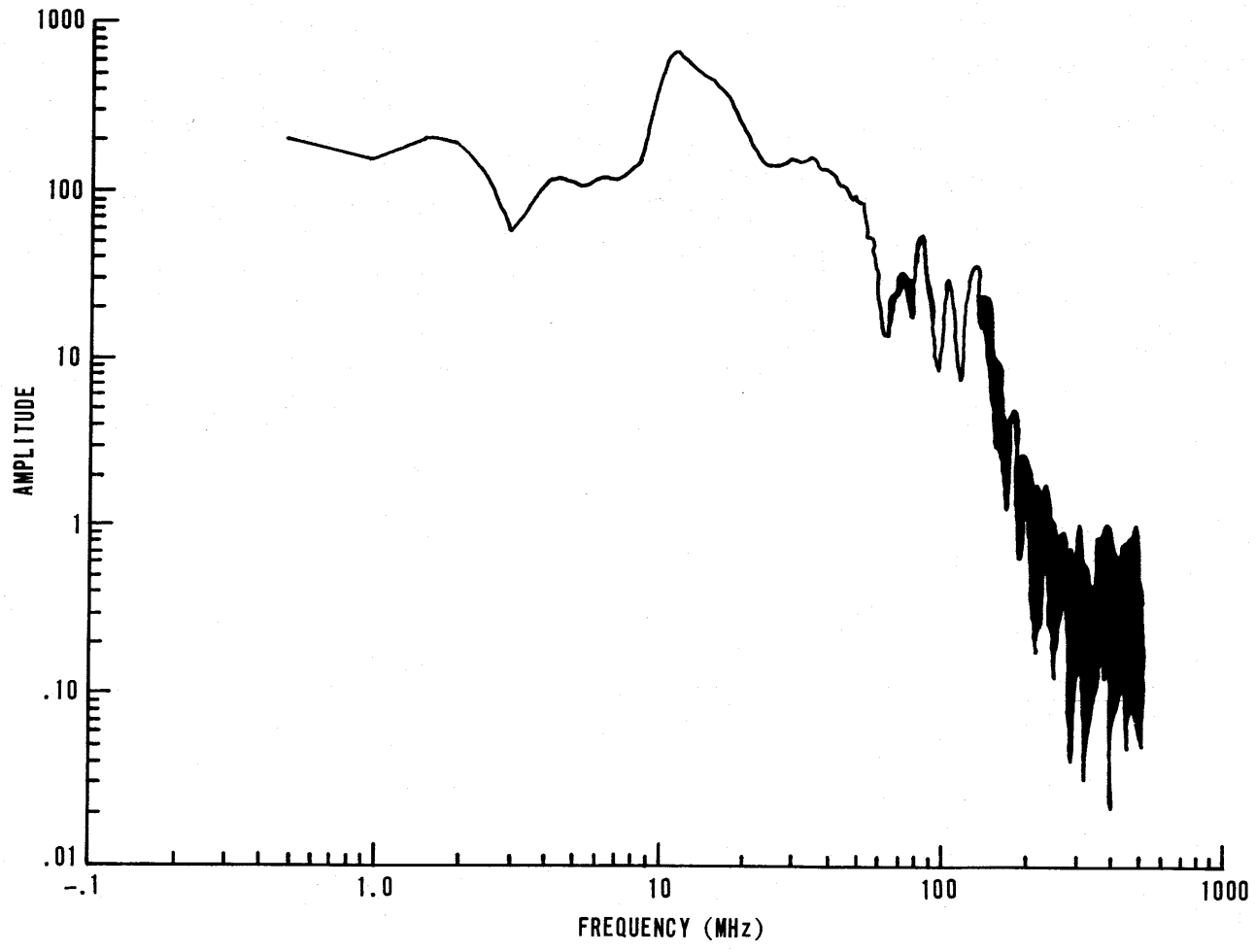

Figure 3. Response Transform Magnitude, 00,01,00

analysis at 150 ns. The range between 20-50 MHz has no definite peaks. This range is where other pipe response modes should lie, but they evidently damp out quickly with the pipe so near the ground. The poles found for the fourteen shots with T = 8 ns, N = 25 points, M = 5 are plotted in figure 4. The average of these poles is + -.270 ± j 2.20. With each of these shots, two pairs of complex poles and one real positive pole were found. The real pole is the program's attempt to fit the DC offset seen in figure 2. The higher frequency pole pair changed with M, N or T and was judged not to be reliable. The rather small dynamic range in the data after 150 ns limited our ability to find other poles.

The next records analyzed consist of four shots with the pipe at 00, 10, 00. The graph of a typical shot is shown in figure 5 and its corresponding transform in figure 6. From these shots we attempted to find poles from both the pipe response and the incident field. Consequently the analysis was started at time zero. A plot of the poles found is given in figure 7. Real poles were omitted from the plot. Complex poles with frequencies higher than 60 MHz were eliminated by the program. The poles were found with N = 40 points, T = 8 ns, and M = 13 poles. Before analysis, each record was filtered with a two-pole Butterworth filter having a cutoff frequency of 60 MHz. The sample spacing for the filter operation was 1 ns. The filter did not greatly affect the three low frequency pole pairs. We were not able to get good results for the higher frequency poles without the filter. As expected, the best grouping occurs for the poles corresponding to the highest peaks in figure 6. The remaining poles group well in frequency but poorly along the $\sigma L/c$ axis.

With the pipe at 00, 10, 00 the situation is much different than at 1 meter. First, the lowest frequency pole pair has shifted normalized frequency from approximately 2.20 to 2.00. And second, there are a number of other pairs. To sort out which of these poles are from the pipe response and which from the incident field we need to analyze the incident field.

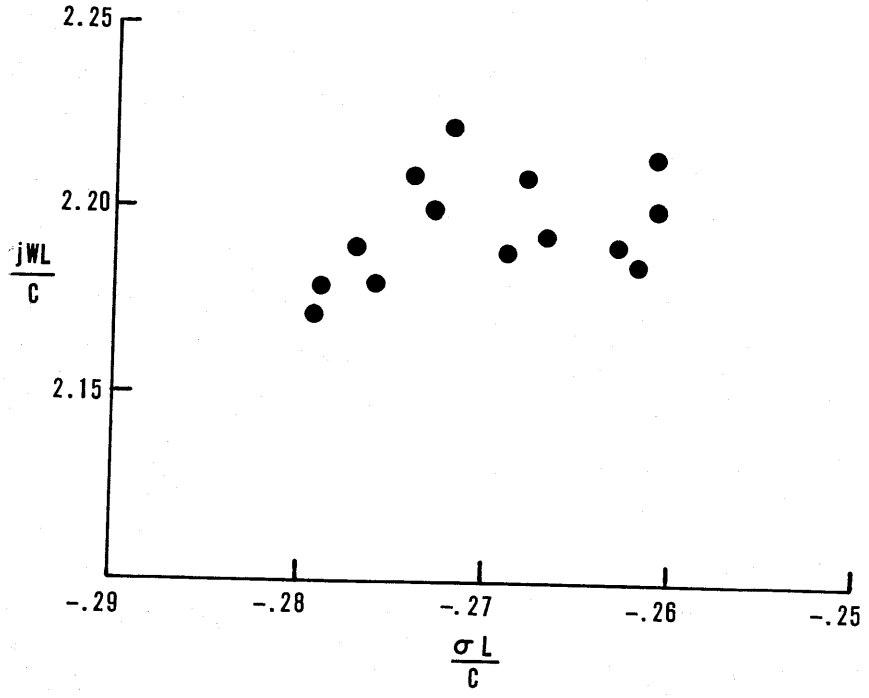

Figure 4. Pole Locations 00, 01, 00 (14 shots)

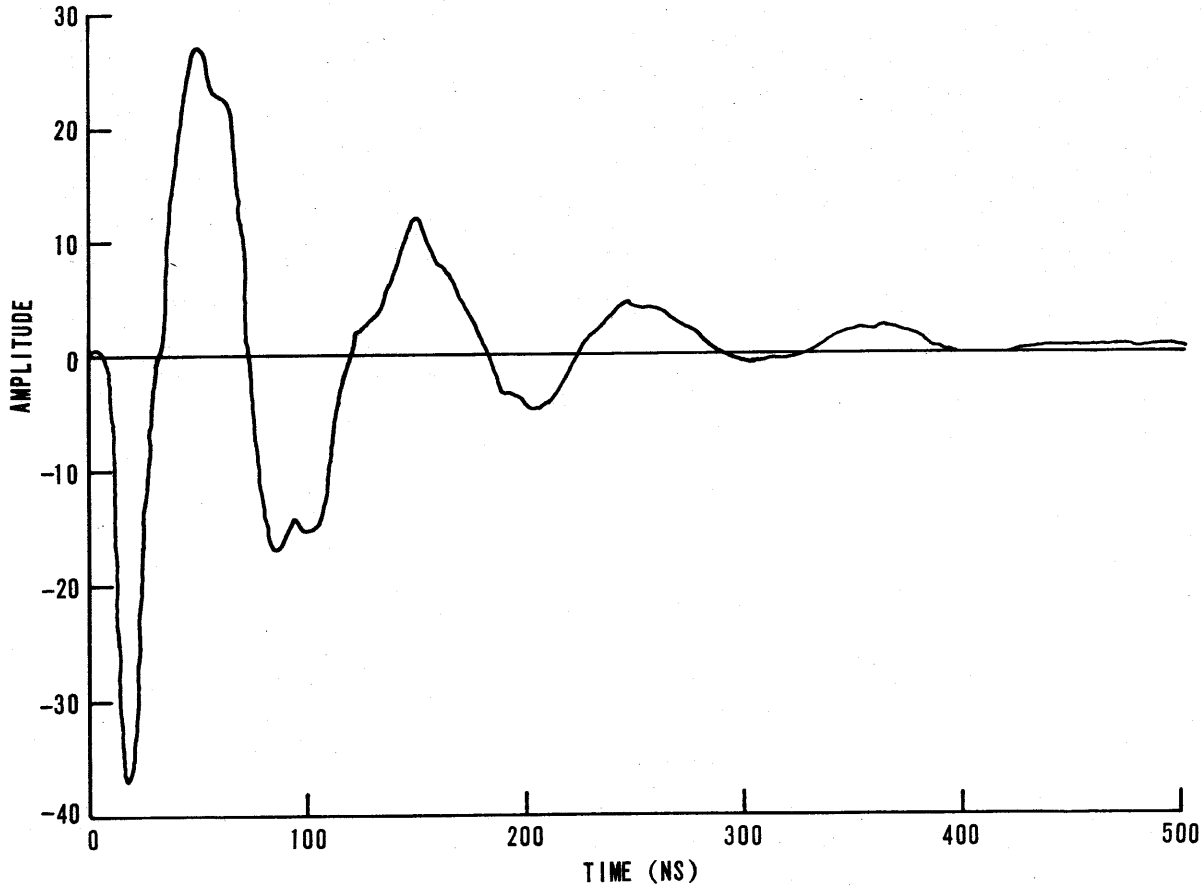

Figure 5. $\dot{J}_A$ Response at 00, 10, 00

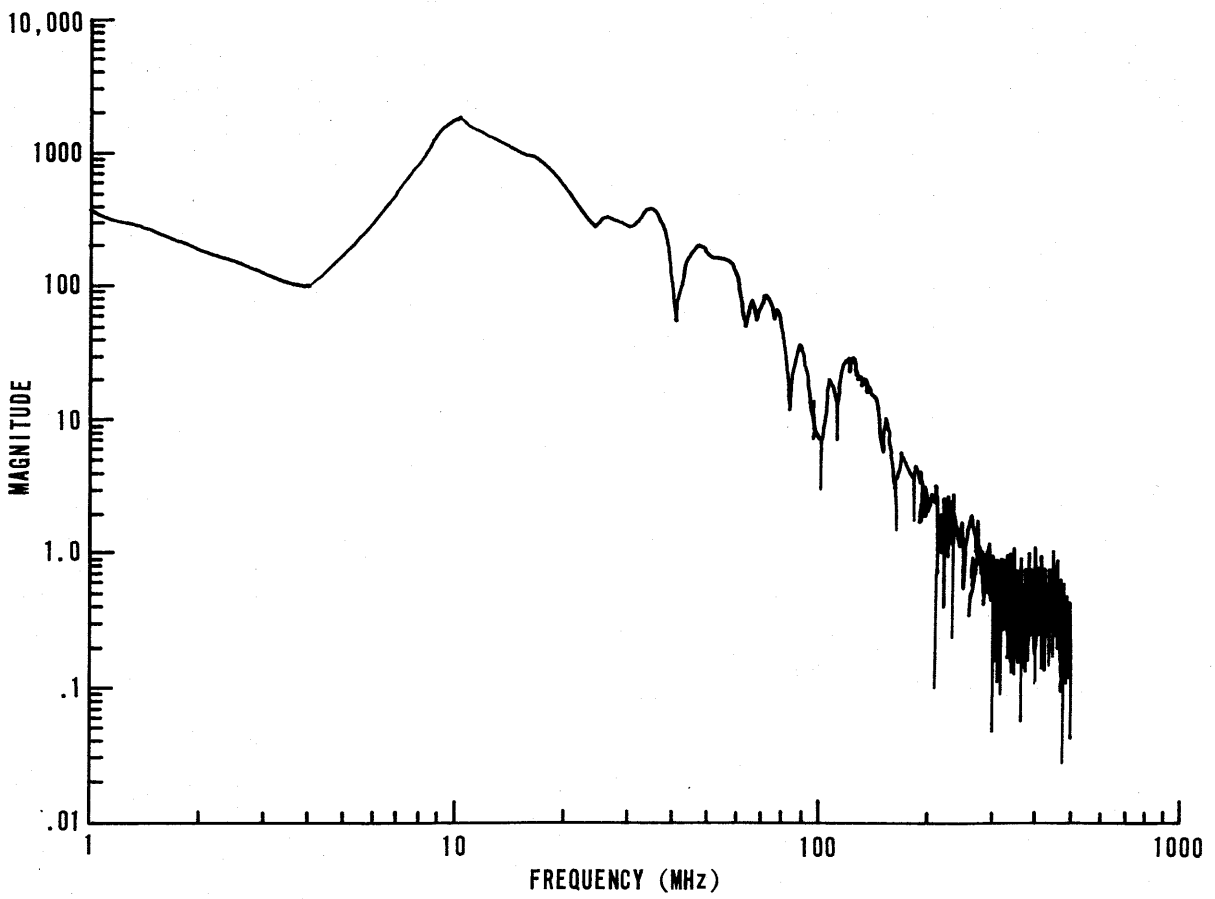

Figure 6. $\dot{J}_A$ Response Transform Magnitude 00,10,00

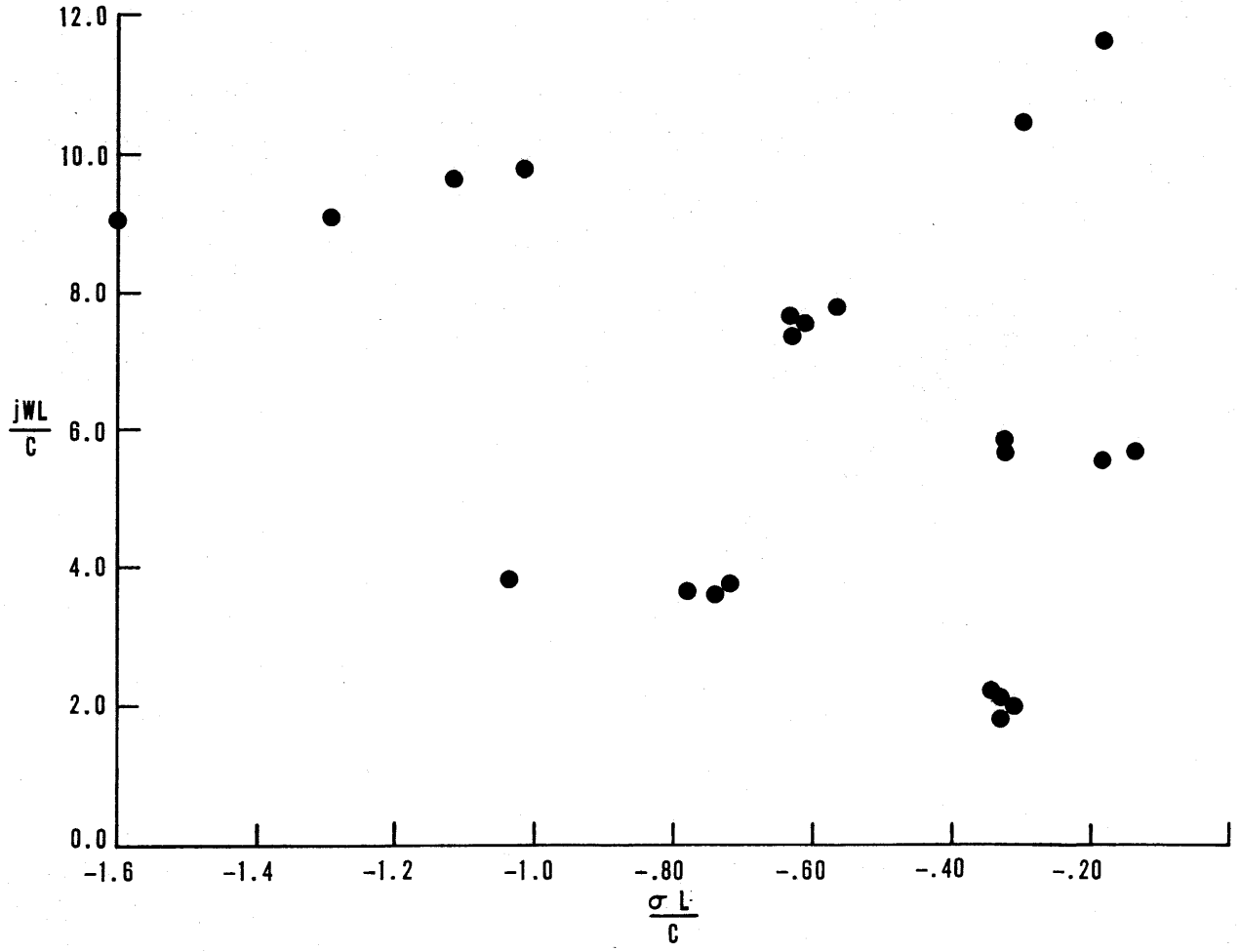

Figure 7. Pole Locations 00,10,00 (4 shots)

Figure 8 is a graph of the incident H_Z field at 00,09,00. The 9 m height is as close to 10 m as the field map data comes. The total incident field consists of a direct wave plus a reflection from the ground plane. The superposition of these two waves accounts for most of the peaks and nulls in the H_Z spectrum at frequencies below 60 MHz that are evident in figure 9. Reference 10 has an analysis of this reflection effect.

Table 1 lists the poles found from the H_Z record. These poles are compared with the poles found from the total pipe response at 00,10,00. The H_Z record was low-pass filtered and then analyzed using N = 40 points, M = 17 poles, and T = 8 ns sample spacing. The analysis began at time zero. Because of the reflection, the Laplace transform of the measured response is in the form $R(s) = [1 + K\exp(-s\tau)]\ F(s)$ where F(s) is the response to the direct wave, τ is the delay between arrival of the direct and reflected wave, and K is the reflection coefficient. If we take K = 1 as the simplest case then the magnitude of the response Fourier transform can be written as

$$|R(jw)| = 2\left|\cos \frac{w}{2} \tau\right| \ |F(jw)| \qquad (19)$$

The poles of R(s) consist of the poles of F(s) plus poles used to approximate the $[1 + K\exp(-s\tau)]$ term. Equation (19) indicates that these poles should have frequencies that are multiples of $1/2\tau$. With the field sensor at 00,09,00 a null should occur at $1/2\tau$ = 8.33 MHz. This is a normalized frequency of 1.74 which is in good agreement with the measured value listed in table 1. By an interesting coincidence, the width of the incident field pulse is about 60 ns. Because of this, the peaks and nulls in the field spectrum produced by the fundamental pulse will tend to coincide with those produced by the reflection effect.

From the data it appears that the pole pair $-.346 \pm j\ 2.02$ corresponds to the first pipe natural resonance. The pole pair $-.528 \pm j\ 5.11$ may be due to the second pipe resonance. The

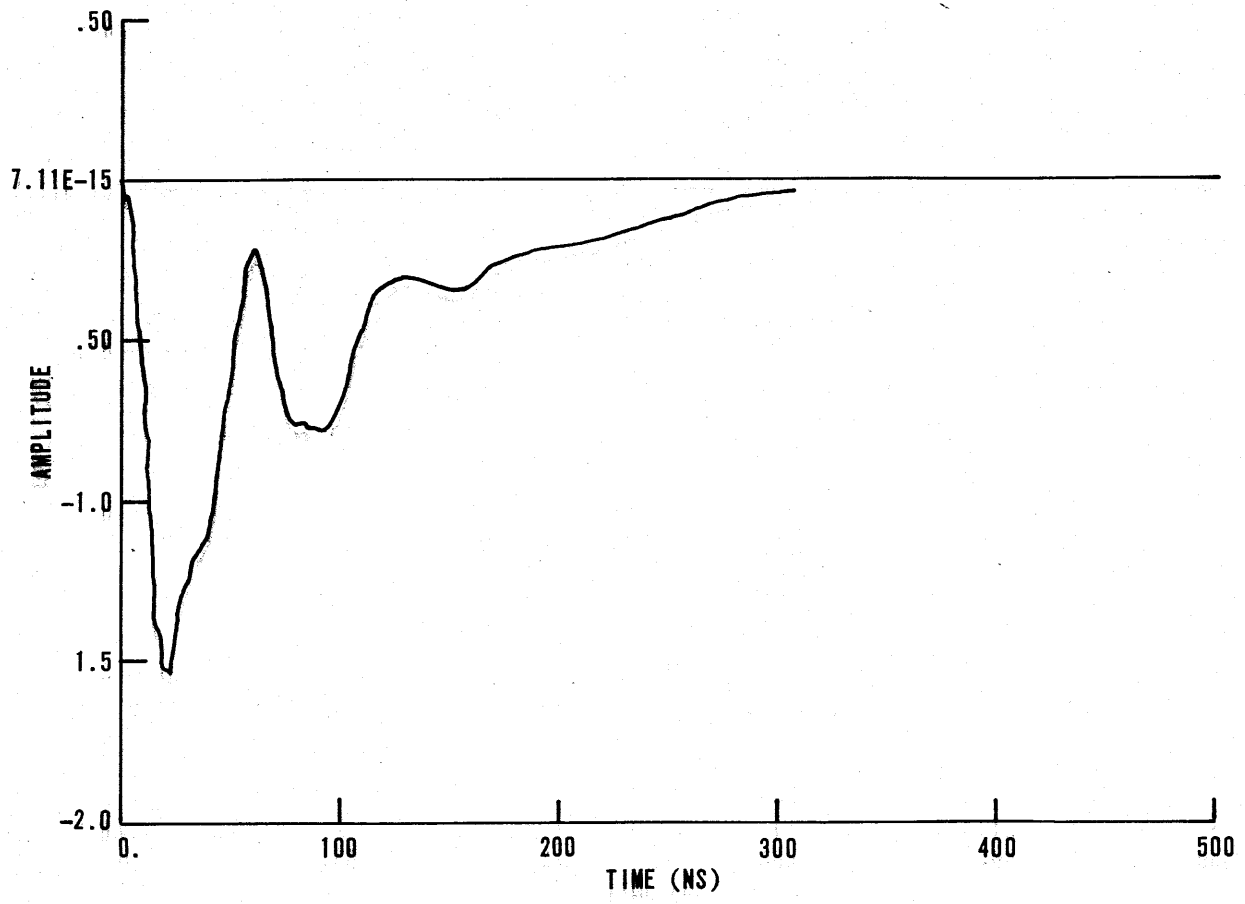

Figure 8. Incident Field H_Z, 00,09,00

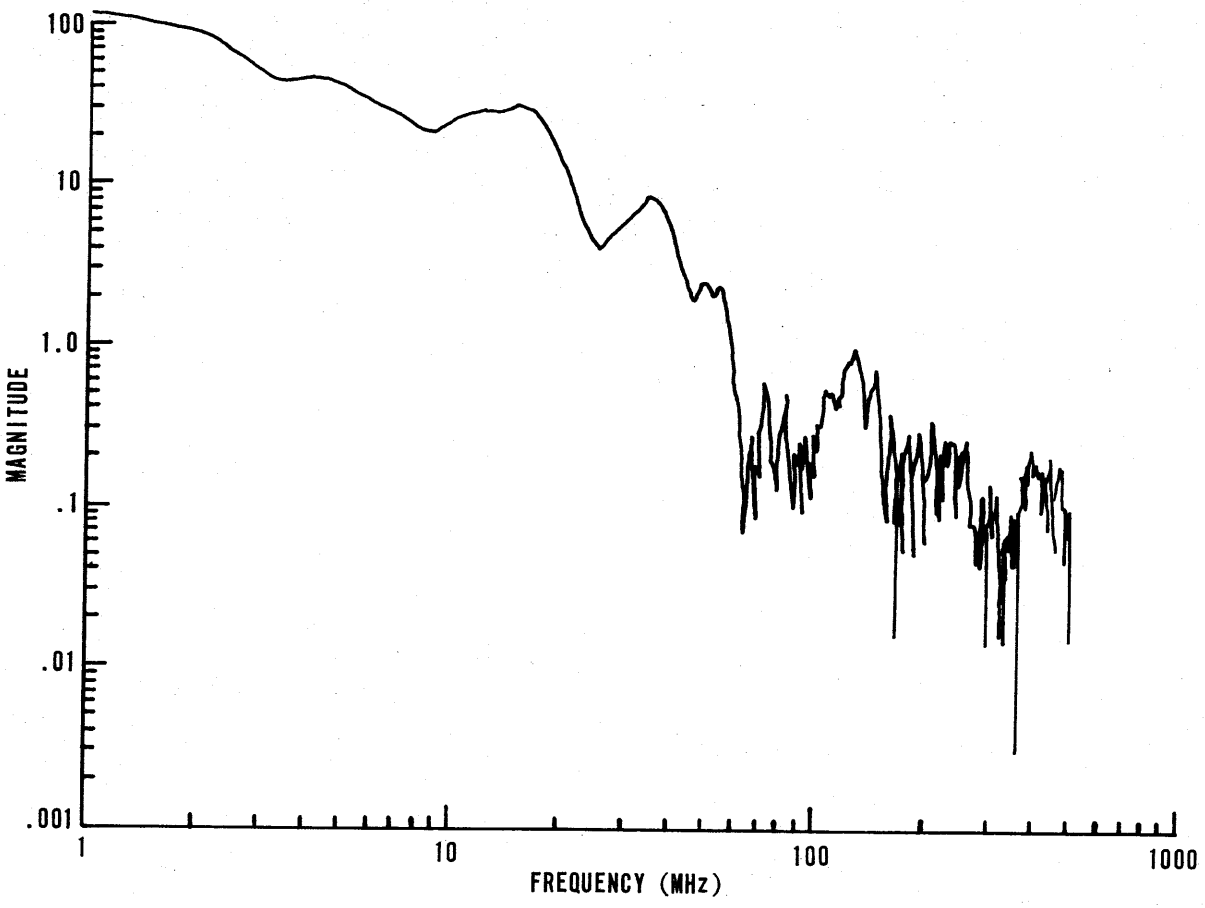

Figure 9. H_Z Transform Magnitude 00,09,00

Table 1

INCIDENT FIELD AND RESPONSE POLES

Incident Field Poles	Pipe Response Poles
H_z at 00,09,00	$\dot{J}_A$ at 00,10,00
ADN 0200809	PH 00416
-.137 ± j 1.73	-.346 ± j 2.02
-.663 ± j 3.42	-.545 ± j 3.54
-.867 ± j 5.79	-.528 ± j 5.11
-.698 ± j 6.76	-.546 ± j 6.70
-.373 ± j 8.01	-.577 ± j 8.05
-.710 ± j 9.74	-1.11 ± j 10.5

results are inconclusive on this point since the incident field has a nearby pole pair at $-.867 \pm j\ 5.79$ which is only about 13% different in frequency. The remaining poles listed in table 1 match the incident field poles fairly well in frequency. Moreover, except for the pair $-.867 \pm j\ 5.78$, the incident field pole frequencies match the peaks and nulls in the Fourier transform magnitude seen in figure 9. From the results described so far it is possible to make two conclusions: first, there is a significant change in the fundamental frequency when the pipe is raised from 1 m to 10 m, and second, most (and maybe all) of the higher than fundamental frequency poles found in the 10 m data are due to the incident field.

The next records analyzed were of $\dot{J}_A$ at 00,01,30. Two shots were run starting at 75 ns, each with N = 37 points, M = 7 poles, and T = 7.8 ns sample interval. The only numerically stable pole pair (that is insensitive to change in N, M, T or starting time) was $-.267 \pm j\ 2.19$ for record PH00077 and $-.275 \pm j\ 2.16$ for record PH00156. The average $-.271 \pm j\ 2.17$ agrees well with the average $-.270 \pm j\ 2.20$ of the fourteen shots at 00,01,00. This indicates that, as expected, moving the pipe along the Z-axis while holding (X,Y) = (00,01) does not greatly affect the location of the natural response. Ground reflections are not important with the pipe so close to the ground.

The last data discussed here consists of 3 shots at 00,10,30. The time domain graph of one of these shots is shown in figure 10 and the Fourier transform magnitude in figure 11. A comparison of the incident field and pipe response poles is given in table 2. A plot of the poles found from all three shots is given in figure 12. The analysis was done starting at time zero with N = 40 points, M = 13 poles, and T = 8 ns sampling interval. Each record was filtered with a two-pole low-pass Butterworth filter having a 3 db point at 60 MHz.

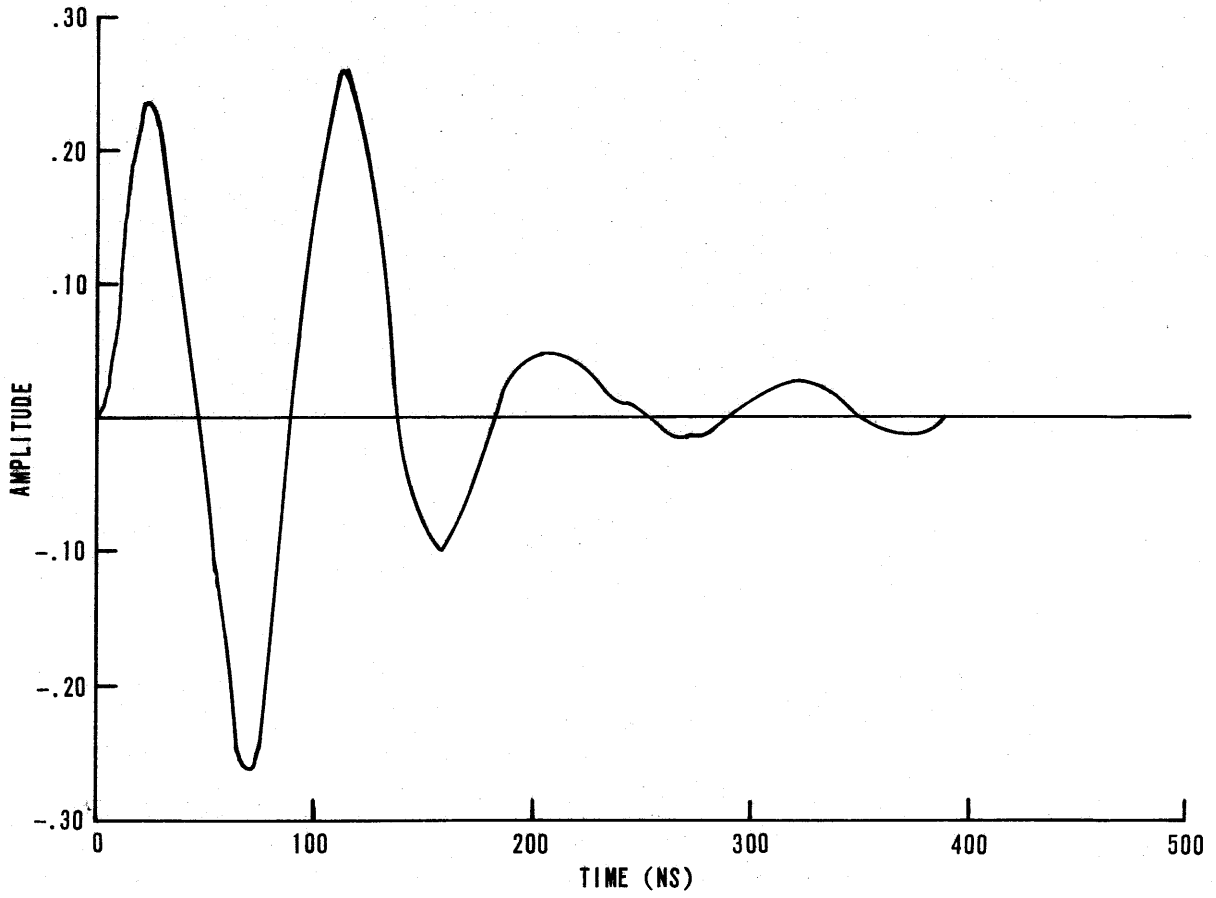

Figure 10. $\dot{J}_A$ Response at 00,10,30

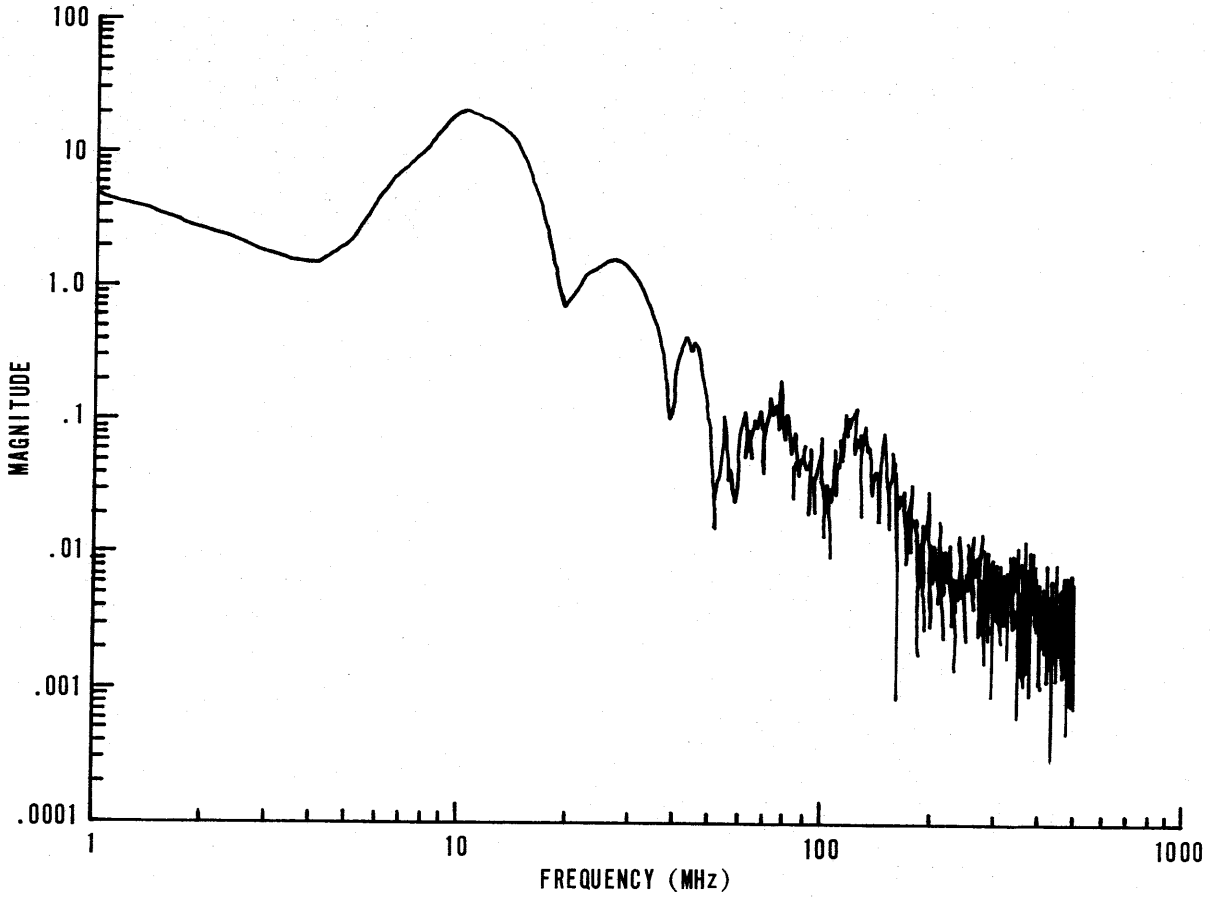

Figure 11. $\dot{J}_A$ Response Transform Magnitude 00,10,30

Table 2

INCIDENT FIELD AND RESPONSE POLES

Incident Field Poles	Pipe Response Poles
H_z at 00,09,30	$\dot{J}_A$ at 00,10,30
ADN 0202070	PH00146
-.641 ± j 1.72	--
--	-.422 ± j 2.03
-.744 ± j 3.40	-.559 ± j 3.03
-.104 ± j 5.87	-.608 ± j 5.56
-.403 ± j 7.11	-.971 ± j 7.47
-.912 ± j 9.07	-.937 ± j 9.39

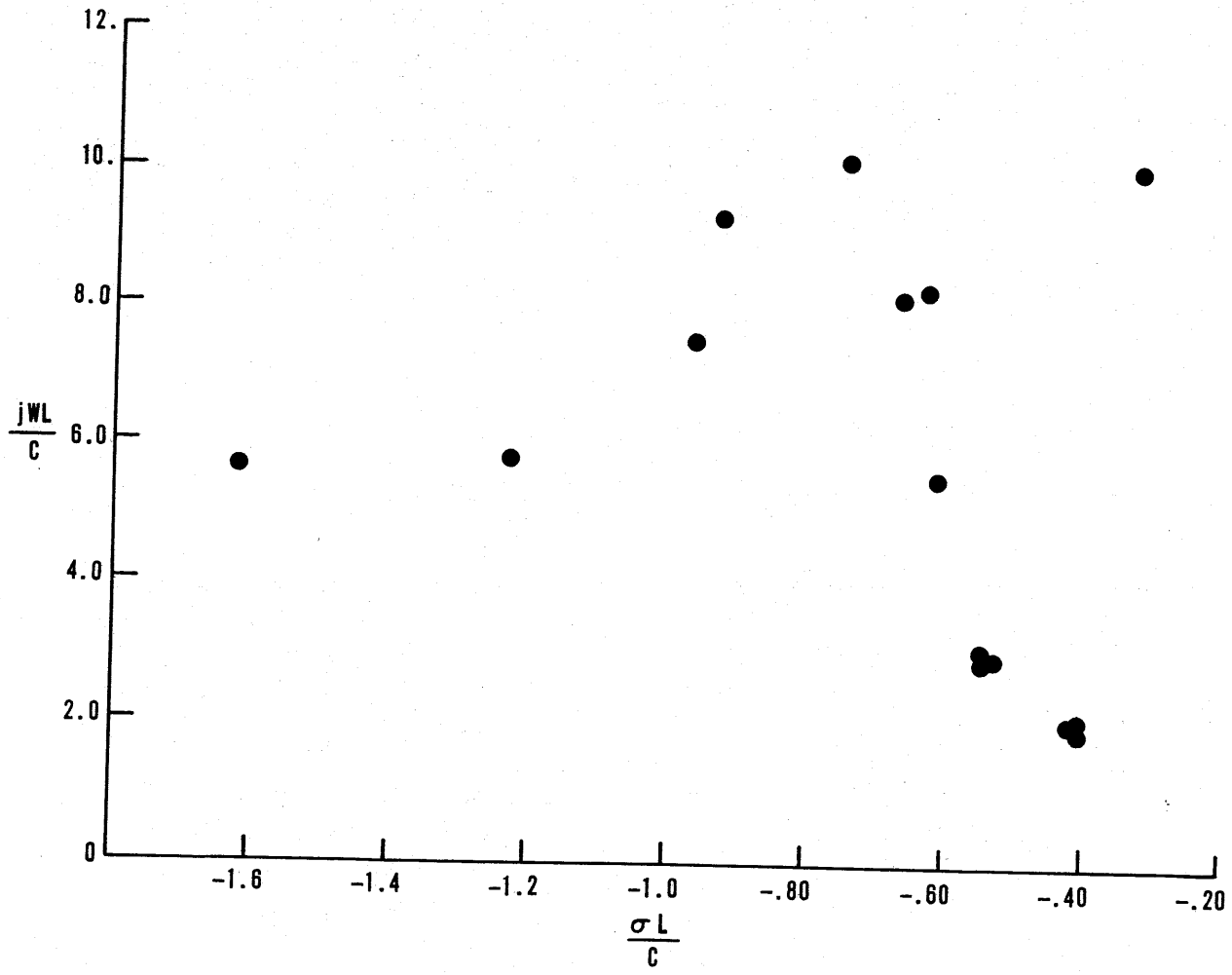

Figure 12. Pole Locations 00,10,30 (4 shots)

The incident field and pipe response poles shown in Table 2 do not agree as well as those in Table 1. The pair -.422 ± j 2.03 is the first pipe natural frequency. Recall that the measurement at 00,10,00 gave this singularity as -.346 ± j 2.02. The frequencies agree well. The variation in real part may be due to some asymmetry in the ground plane. We would like to say that the remaining poles in the pipe response are due to the incident field. For location 00,10,30 the delay time between the direct and reflected waves is τ = 46.5 ns. The graph of H_z in figure 13 indicates that this is a correct value. According to equation (19) the first null in the spectrum of H_z should be at $1/2\tau$ = 10.7 MHz. Figure 14 shows nulls at approximately the odd harmonies of 10.7 MHz. So the simple reflection theory used to derive equation (19) is adequate to explain the general shape of the incident field spectrum.

The frequencies of the first two incident field pole pairs listed in table 2 for 00,09,30 match the field poles in table 1 for 00,09,00. This indicates that these poles are due to the shape of the pulser output and not to reflections. The response pole pair -.559 ± j 3.03 doesn't match any of the incident field poles very well. But its frequency corresponds to a peak in the pipe response (figure 11). The frequencies of the remaining incident field and pipe response poles agree to within about 5%. Overall, the results at this location have more unexplained variation than at the other three locations.

The residues corresponding to the poles described above for the two 10 m high locations are listed in table 3 for reference.

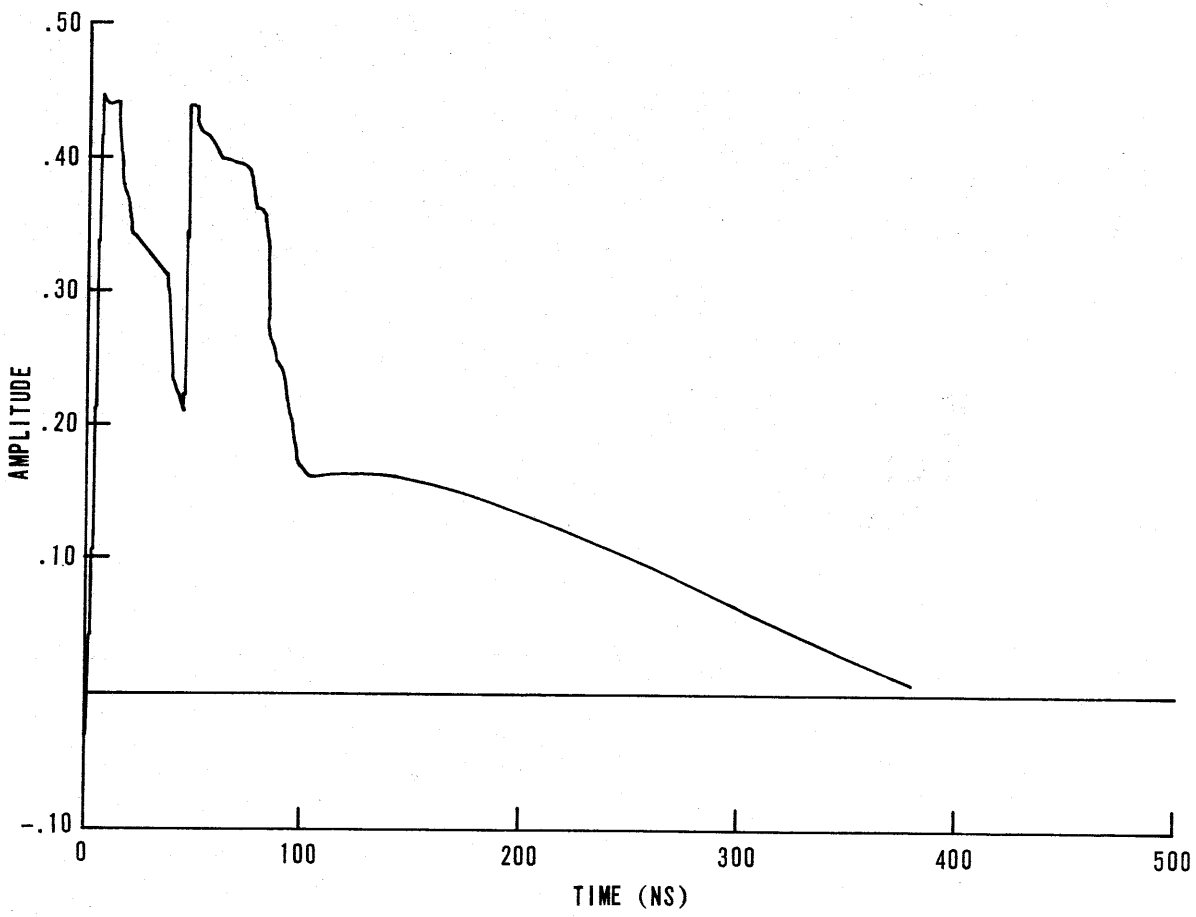

Figure 13. Incident Field, H_Z 00,09,30

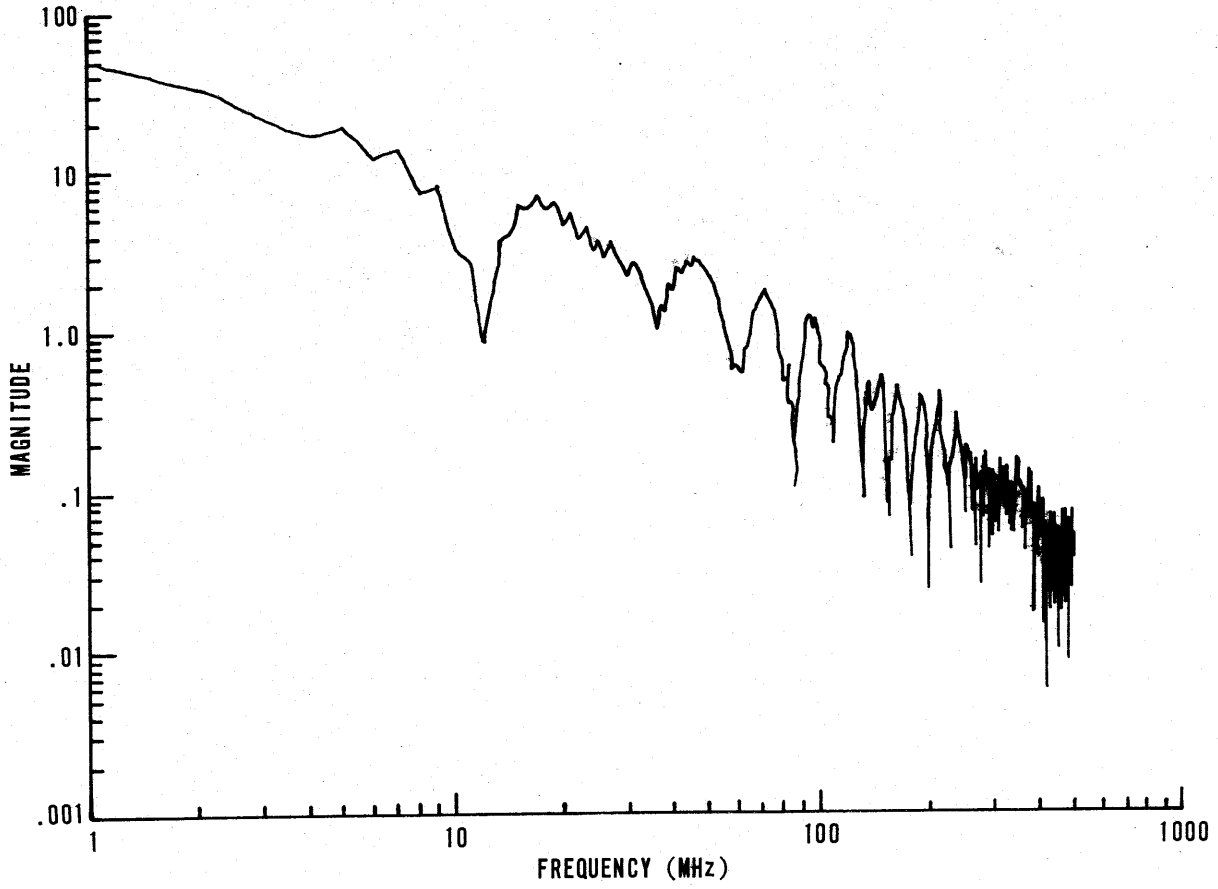

Figure 14. Transform Magnitude, Incident Field H_z, 00-09-30

Table 3

POLES AND RESIDUES

PH00416 Location 00,10,00, $\dot{J}_A$

Poles	Residues
-.346 + j 2.02	-17.8 - j 11.2
-.545 + j 3.54	5.50 + j 4.61
-.528 + j 5.11	-1.53 + j .0001
-.546 + j 6.70	-.452 + j 1.25
.577 + j 8.05	-3.72 - j 3.56
-1.11 + j 10.5	-2.47 - j 6.73

PH00146 Location 00,10,30, $\dot{J}_A$

-.422 + j 2.03	248. - j 48.2
-.551 + j 3.03	-123. + j 101.
-.608 + j 5.56	-8.66 - j 2.94
-.971 + j 7.47	18.2 + j 19.1
-.937 + j 9.39	-3.45 + j 13.8

SECTION 4
CONCLUSIONS

In trying to assess the reliability of poles extracted from experimental data the following three tests are useful:

1. The poles found from different shots at the same location should group well;
2. The poles calculated should vary by only a few percent when N, M, or T are changed within the limits imposed by the available data;
3. The pole frequencies should correspond to structure in the Fourier transform magnitude.

The poles corresponding to the fundamental pipe resonance pass these tests. All the other poles are less reliable. The reason of course is that most of the signal energy is in the fundamental component. The higher order poles satisfy the tests above if the imaginary part only is considered. Unfortunately the real parts fail the first two tests. Our experience with computer generated data has been that the real part of poles is more sensitive to noise than the imaginary part. With these warnings about the real parts of the higher order poles, we can make the following conclusions.

Most of the peaks and nulls in the incident H_z fields can be explained by the reflection effect. The first two singularities are the same at 00,09,00 and 00,09,30 even though the path difference is not the same. From this we can conclude that these poles are due to the shape of the field pulse and not the interaction of two pulses due to reflection.

It appears that the structure of the pipe response can be accounted for by the superposition of the fundamental mode response due to the direct and to the reflected fields. That is, it does not appear that any of the higher order pipe modes were excited a measurable amount. The agreement between the incident field poles

and pipe response poles is only fair. There are at least four reasons for this:

1. The poles that don't agree well correspond to parts of the spectrum where the signal to noise ratio is low;
2. The field map and pipe response data were taken at different heights;
3. The poles in question are the result of the method's attempt to approximate the [1 + Kexp(-sτ)] term which is not a rational function of s; and
4. The pipe response depends on the incident fields over all the pipe surface while the incident field measurement depends on the smaller sensor surface.

It is interesting to compare the measured poles with some calculated values. Strictly speaking the results of references 2 and 3 do not apply to the lossy ground plane case at the HPD facility so we cannot expect close agreement. For a cylinder in free space with length to radius ratio of 20, Shumpert[2] gives $-.44 \pm j\ 2.5$ as the first singularities. With the cylinder 1 m above a perfectly conducting ground plane he computed $-.056 \pm j\ 2.75$. Marin[3] has $-.05 \pm j\ 2.90$ for parallel cylinders 2 m apart and $-.417 \pm j\ 2.90$ for parallel cylinders 20 m apart. Taken together, these results predict that as the distance from cylinder to ground plane increases the pole real part increases. Other results in reference 3 indicate that the imaginary part should decrease. The measured results presented in this report bear out these predictions. However, the measured frequencies at both 1 m and 10 m are much lower than predicted and the damping is higher. We can suspect that these differences are due to losses in the ground plane.

REFERENCES

1. C. E. Baum, "On the Singularity Expansion Method for the Solution of Electromagnetic Interaction Problems," Interaction Note 88, 11 Dec 1971.

2. T. H. Shumpert and D. J. Galloway, "Transient Analysis of a Finite Length Cylindrical Scatterer Very Near a Perfectly Conducting Ground," Sensor and Simulation Note 226, August 1977.

3. L. Marin, "Natural Modes of Certain Thin-Wire Structures," Interaction Note 186, August 1974.

4. K. J. Astrom and P. Eykhoff, "System Identification--A Survey," Automatica, Vol. 7, 1971.

5. M. L. Van Blaricum and R. Mittra, "Techniques for Extracting the Complex Resonances of a System Directly from its Transient Response," Interaction Note 301, December 1975.

6. A. G. Evans and R. Fischl, "Optimal Least Squares Time-Domain Synthesis of Recursive Digital Filters," IEEE Trans. on Audio and Electroacoustics, Vol. AU-21, February 1973.

7. C. L. Lawson and R. J. Hanson, Solving Least Squares Problems, Prentice-Hall, 1974.

8. K. Steiglitz and L. E. McBride, "A Technique for the Identification of Linear Systems," IEEE Trans. on Automatic Control, Vol. AC-10, October 1965.

9. K. Steiglitz, "On the Simultaneous Estimation of Poles and Zeros in Speech Analysis," IEEE Trans. on Acoustics Speech and Signal Processing, Vol. ASSP-25, June 1977.

10. J. P. Castillo and B. K. Singaraju, "Effects of Wave Reflection on Objects Near a Plane Ground," ATHAMAS Memo 8, May 1975.